

Research Paper

Endothelial PPAR δ facilitates the post-ischemic vascular repair through interaction with HIF1 α

Yalan Wu^{1,2}, Xiaolong Tang^{3,4}, Sharen Lee¹, Huiling Hong^{1,2}, Xiaoyun Cao^{1,2}, Chi Wai Lau¹, Baohua Liu^{3,4}, Ajay Chawla⁵, Ronald Ching Wan Ma⁶, Yu Huang^{1,2}, Kathy O Lui^{2,7}, Xiao Yu Tian^{1,2}✉

1. School of Biomedical Sciences, Faculty of Medicine; Chinese University of Hong Kong, Hong Kong SAR, China.
2. CUHK Shenzhen Research Institute, Shenzhen, China.
3. Shenzhen Key Laboratory for Systemic Aging and Intervention (SAI), National Engineering Research Center for Biotechnology (Shenzhen), International Cancer Center, Shenzhen University, Shenzhen, China.
4. Guangdong Key Laboratory of Genome Stability and Human Disease Prevention, Department of Biochemistry & Molecular Biology, School of Basic Medical Sciences, Shenzhen University, Shenzhen, China.
5. Department of Physiology, Department of Medicine, University of California San Francisco, CA 94143, United States.
6. Department of Medicine and Therapeutics, Li Ka Shing Institute of Health Sciences, Hong Kong Institute of Diabetes and Obesity, The Chinese University of Hong Kong, Prince of Wales Hospital, Hong Kong, SAR, China.
7. Department of Chemical Pathology, Li Ka Shing Institute of Health Sciences, Chinese University of Hong Kong, Hong Kong SAR, China.

✉ Corresponding author: Xiao Yu TIAN, School of Biomedical Sciences, Room 208, LIBSB, Area 39, Chinese University of Hong Kong, Shatin, NT, Hong Kong SAR, China. Tel: 852-39433075; Fax: 852-26035123; Email: xytian@cuhk.edu.hk

© The author(s). This is an open access article distributed under the terms of the Creative Commons Attribution License (<https://creativecommons.org/licenses/by/4.0/>). See <http://ivyspring.com/terms> for full terms and conditions.

Received: 2021.11.13; Accepted: 2021.12.10; Published: 2022.01.24

Abstract

Rationale: Restoration of vascular perfusion in peripheral arterial disease involves a combination of neovessel formation and the functional restoration of vascular endothelium. Previous studies indicated that ligand-dependent PPAR δ activation enhances angiogenesis. However, how PPAR δ is triggered by hypoxia and its downstream effects during post-ischemic vascular repair was not well understood.

Methods: We induced experimental hindlimb ischemia in endothelial cell selective *Ppard* knockout induced by *Cdh5-Cre* mediated deletion of floxed *Ppard* allele in mice and their wild type control and observed blood perfusion, capillary density, vascular relaxation, and vascular leakage.

Results: Deletion of endothelial *Ppard* delayed perfusion recovery and tissue repair, accompanied by delayed post-ischemic angiogenesis, impaired restoration of vascular integrity, more vascular leakage and enhanced inflammatory responses. At the molecular level, hypoxia upregulated and activated PPAR δ in endothelial cells, whereas PPAR δ reciprocally stabilized HIF1 α protein to prevent its ubiquitin-mediated degradation. PPAR δ directly bound to the oxygen-dependent degradation domain of HIF1 α at the ligand-dependent domain of PPAR δ . Importantly, this HIF1 α -PPAR δ interaction was independent of PPAR δ ligand. Adeno-associated virus mediated endothelium-targeted overexpression of stable HIF1 α *in vivo* improved perfusion recovery, suppressed vascular inflammation, and enhanced vascular repair, to counteract with the effect of *Ppard* knockout after hindlimb ischemia in mice.

Conclusions: In summary, hypoxia-induced, ligand-independent activation of PPAR δ in ECs stabilizes HIF1 α and serves as a critical regulator for HIF1 α activation to facilitate the post-ischemic restoration of vascular homeostasis.

Key words: Endothelial cell, PPAR δ , HIF1 α , hindlimb ischemia, vascular homeostasis

Introduction

Peripheral artery disease (PAD) of the lower limbs is the third leading cause of atherosclerotic cardiovascular disease after coronary artery disease and stroke [1]. Critical limb ischemia is the most

severe form of PAD which could lead to ulcer, gangrene, and amputation. Although there are effective therapies to lower the cardiovascular risk and to prevent the progression to critical limb

ischemia, patients with PAD continue to be under-recognized and undertreated. Many efforts have been made to enhance lower-extremity blood flow via therapeutic angiogenesis for patients with PAD [2]. In addition, there has been much interest in the use of stem cell-derived endothelial cells or modification of resident stem cells [3]. However, interventions for severely ischemic PAD patients are still very limited besides endovascular procedures and surgeries to rebuild blood flow. It is important to identify critical endogenous regulators and explore approaches to enhance their function in vivo in order to enhance post-ischemic vascular recovery.

To date, several important transcription factors have been identified for post-ischemic vascular recovery, including KLF5, ETS1, COUP-TFII, etc. [4]. Many of these transcription factors regulate post-ischemic angiogenesis through expression of growth factors VEGFs, PDGFs, and their receptors. For example, ETV2 mediates VEGFR2 expression and contributes to neovascularization after hindlimb ischemia injury [5]. TFEB also facilitates angiogenesis through activation of AMPK and autophagy [6]. Importantly, expression of HIF1 α after ischemia is a critical event for the induction of angiogenic factors, as well as mobilization of angiogenic cells [7]. Reducing HIF1 α inactivation could improve angiogenesis in ischemic muscle [8]. In addition, the stability of HIF1 α is also modulated by many factors, including enzymes such as heme oxygenase-1 and glutaredoxin-1 during post-ischemic angiogenesis [9, 10]. Modulating HIF1 α activity and identifying its interacting factors could provide some hint for developing therapies to improve perfusion.

The peroxisome proliferator-activated receptors (PPARs) are ligand-activated transcription factors in which three distinct isoforms (PPAR- α , - γ , and - δ) have been identified in tissues. Previous studies demonstrated the protective role of PPAR δ agonists in the cardiovascular system against atherosclerosis, stroke, aortic aneurysm, diabetic vasculopathy, etc. [11-13]. PPAR δ agonist also inhibits vascular inflammation and reduces atherosclerotic lesions in mouse models [11, 14-16]. Early studies suggested that PPAR δ agonists, such as GW501516 enhance angiogenesis of human endothelial cells in vitro [17]. Prostacyclin also promotes the pro-angiogenic function of human endothelial progenitor cells in a PPAR δ -dependent manner [18]. Likewise, PPAR δ agonists enhance the regenerative capacity of human endothelial progenitor cells [19, 20], and also protect endothelial cells from apoptosis [21]. These observations suggest that ligand-induced PPAR δ activation may play a positive role in vascular homeostasis while the detailed mechanism and

regulation is yet to be better understood.

In this study, we have showed that endothelial expression of PPAR δ regulates several aspects of vascular homeostasis by enhancing post-ischemic angiogenesis, and endothelial barrier function, while inhibiting endothelial activation and inflammatory responses. We also showed an important role of hypoxia-induced PPAR δ , which reciprocally enhances HIF1 α stability and its downstream target genes participating in the vascular repair and restoration of vascular integrity. The interaction and regulation of PPAR δ -HIF1 α is critical for perfusion recovery in hindlimb ischemia.

Methods

Animals

All the mice were housed at 22 °C in a barrier facility and kept on a 12-hour light, 12-hour dark cycle with free access to food and water. The *Ppard* floxed mutant mice (B6.129S4-*Ppard*^{tm1Rev}/J) and the VEC-cre transgenic mice (B6;129-Tg(*Cdh5-cre*)^{1Spe}/J) were originally from Jackson laboratory. Both strains were backcrossed with C57BL/6 mice before they were crossed to generate endothelial cells specific deletion of *Ppard* as *Ppard*^{f/f};*Cdh5*^{Cre/+} (*Ppard*^{EC-KO}) mice. Their wild type controls were *Ppard*^{f/f} (*Ppard*^{EC-WT}) mice. Mouse genotype were validated by DNA genotyping using Jax protocols, mRNA and protein expression. All the experiments were performed using littermates, which were randomized to experimental groups. The observers of mouse experiments and analysis were blinded with genotype information, which was matched afterwards.

Hindlimb ischemia model and assessments

Hindlimb ischemia (HLI) was induced by ligation of femoral artery in male mice at 10–12 weeks of age. Mice were anesthetized via intraperitoneal injection of a combination of 75 mg/kg ketamine and 10 mg/kg xylazine (Alfasan Co, Netherlands) before the unilateral ligation was performed. In this unilateral ischemia model, the contralateral limb was considered as a control. Mice were kept warm on a heatpad at 36 \pm 1.0 °C during the procedure. Blood perfusion was measured by imaging of plantar regions of interests with Laser Doppler Imager (Moor Instruments) and the average lower leg blood flow was presented as the ratio of ischemic to non-ischemic side at days 0, 3, 7, 14, 21 and 28 following HLI. Vasculature imaging of the thigh was performed with the Laser Speckle Contrast Imaging System RFLSI III (RWD Life Science Co.).

Histological analysis

GA muscle was embedded in OCT and frozen in

cooled 2-methylbutane. Frozen section was cut at 10 μm . Sections were fixed with 4% paraformaldehyde, washed in PBS, and stained with hematoxylin and eosin. Some sections were fixed in Mordant in Bouin's solution for 30 min, stained sequentially with Weigert's iron hematoxylin, Biebrich scarlet-acid fuchsin, phosphotungstic/phosphomolybdic acid, and aniline blue. Sections were washed, dehydrated, and mounted with a xylene-based mounting medium.

Functional assay by wire myograph

After mice were euthanized by CO_2 inhalation, femoral arteries were removed and placed in oxygenated ice-cold Krebs solution that contained (mmol/L) 119 NaCl, 4.7 KCl, 2.5 CaCl_2 , 1 MgCl_2 , 25 NaHCO_3 , 1.2 KH_2PO_4 , and 11 D-glucose. Changes in isometric tone of the femoral arteries were recorded in wire myograph (Danish Myo Technology, Aarhus, Denmark). The vascular segments were stretched to an optimal baseline tension of 0.8-1 mN and then allowed to equilibrate for 1 h before the experiment commenced. Segments were first contracted with 60 mmol/L KCl and rinsed in Krebs solution. After several washouts, phenylephrine (10 $\mu\text{mol/L}$) was used to produce a steady contraction, acetylcholine (10 nmol/L to 30 $\mu\text{mol/L}$) was added cumulatively to induce endothelium-dependent vasodilatation on different segments. Endothelium-independent vasodilatation to SNP was performed in the presence of nitric oxide synthase inhibitor L-NAME (0.1 mmol/L), indomethacin (1 $\mu\text{mol/L}$), and 20 mmol/L KCl. Statistical significance was calculated either using the area under curve for each segment or indicated on the individual data points.

RNA isolation and quantitative PCR analysis

Total RNA was extracted from cells or mouse tissues using TRIzol reagent RNAiso Plus (Takara, cat# 9109) and 1 μg of total RNA was reverse transcribed into complementary DNA (cDNA) using 5 \times PrimeScript RT Master Mix (Takara, cat# RR036A), following the manufacturer's instructions. The mRNA levels were determined by quantitative PCR with TB Green[®] Premix Ex Taq[™] (Tli RNase H Plus (Takara, cat# RR420A) detected on an Applied Biosystems ViiA7. All primer sequences are listed in Table S1.

Flow cytometric analysis

At 7 days after HLI surgery, GA muscle from the injured leg was digested with 800 U/ml Collagenase IV + 1 U/ml Neutral Protease (both from Worthington Biochemical) for 60 min. The cells were then suspended in FACS buffer (2% FBS with 2 mmol/L EDTA in PBS), and filtered through 40- μm strainer (BD Biosciences) to generate single-cell suspensions. Cells were firstly incubated with

LIVE/DEAD Aqua (Thermo) for viability following manufacturer's protocol together with anti-CD16/CD32 (10 $\mu\text{g/mL}$, Biolegend) for 30 min. For flow cytometric analysis, cells were then incubated with fluorescent-conjugated anti-mouse antibodies listed in the Table S2. Endothelial cells are defined as $\text{CD45}^- \text{CD31}^+ \text{CD144}^+$. Macrophages are first gated on $\text{CD45}^+ \text{Ly6G}^- \text{CD11b}^+$, and further separated as tissue macrophages ($\text{F4/80}^+ \text{Ly6C}^{\text{lo}}$), and monocyte-derived macrophages ($\text{F4/80}^{\text{mid}} \text{Ly6C}^{\text{hi}}$). Cells were fixed with 1.6% paraformaldehyde for 30 min at 4 $^\circ\text{C}$ until further analysis using FACS Aria Fusion (BD). Data were analyzed using FlowJo.

Immunofluorescence staining

Frozen sections of GA muscle were then fixed in acetone, blocked with normal goat or donkey serum (Abcam), and incubated with primary antibodies and appropriate fluorescence-conjugated secondary antibodies, followed by Hoechst 33342 (Thermo) for nucleus, and mounted in fluorescence mounting medium (Electron Microscopy, Cat#17985-10). Detailed information of all the antibodies used can be found in Table S2.

Lectin injection for vascular structure

After HLI 14 days, functional vessels were stained with fluorescein isothiocyanate (FITC) - Griffonia simplicifolia lectin I (Vector Laboratories, cat#FL-1101-5) (100 $\mu\text{g/mL}$ in PBS) via tail vein injection. Mice were euthanized 5 min after injection and perfused through the heart with PBS followed by 4% paraformaldehyde in PBS. The gastrocnemius muscle was processed for immunofluorescence staining.

Aortic ring assay

Mouse aortic ring assay was performed as previously described [22]. Briefly, the thoracic aortic rings were isolated and 1-mm long aortic rings were embedded in growth factor-reduced Matrigel supplemented with 20 U/mL heparin. The aortic rings were then cultured in Opti-MEM supplemented with 2.5% FBS and 30 ng/mL hVEGF (Peprotech).

Cell culture and cell transfection

Mouse brain microvascular endothelial cells (BMECs, from Angio-Proteomie) were transfected with mouse *Ppard* siRNA (ThermoFisher siRNA ID#151214, #151213), mouse *Hif1a* siRNA (ThermoFisher siRNA ID#158953, #158954) or universal scrambled negative control siRNA using Lipofectamine RNAiMAX Transfection Reagent (Invitrogen), according to the manufacturer's instructions.

Tube formation assays

To examine the effect of *Ppard* knockout on the in vitro angiogenesis of bone marrow derived endothelial cells (BM-ECs). Briefly, a 96-well plate was coated with growth factor-reduced Matrigel (Corning, cat# 354230), which was allowed to solidify at 37 °C for 30 min. BM-ECs (1.8×10^4 per well) were seeded and cultured in EGM-2 medium (Lonza, cat# CC-3202) with 10% FBS under normoxia or hypoxia. The tube-like networks were photographed under a microscope (IX83, Olympus). The perimeters of all the tubes were measured for semi-quantitative analyses using ImageJ Angiogenesis analyzer plug-in as previously described [23].

Plasmids/Transfection

Plasmids transfection was performed by Lipofectamine™ 3000 Transfection Reagent (Thermo Fisher) following the manufacturer's instructions in HEK293T cells and Hela cells. HA-HIF1 α -pcDNA3 (HA-HIF1 α in short, Addgene plasmid #18949; <http://n2t.net/addgene:18949>; RRID: Addgene_18949), and HA-HIF1 α P402A/P564A-pcDNA3 (Addgene plasmid # 18955; <http://n2t.net/addgene:18955>; RRID: Addgene_18955) were gifts from William Kaelin [24]. HIF1 α (401delta603)_R27G (HA- Δ ODD-HIF1 α in short) was a gift from Eric Huang (Addgene plasmid #52215; <http://n2t.net/addgene:52215>; RRID: Addgene_52215) [25]. HRE-luciferase (HRE-Luc in short) was a gift from Navdeep Chandel (Addgene plasmid #26731; <http://n2t.net/addgene:26731>; RRID: Addgene_26731) [26]. Plasmid pcDNA3.1 Flag-HIF1B (#930) was a gift from James Brugarolas (Addgene plasmid #99916; <http://n2t.net/addgene:99916>; RRID: Addgene_99916) [27]. Human *PPARD* was initially amplified from cDNA template and then cloned into p3XFLAG-CMV™-10 (Sigma, E7658) fused with Flag or HA tag. To generate the truncated domains of *PPARD* (Flag-DBD and Flag-LBD) as previously described [28], relevant fragments were amplified by indicated primers listed in **Table S1** and then all were cloned into p3XFLAG-CMV™-10.

Protein extraction and Western blotting

Cells were lysed in 1X SDS lysis buffer [50 mmol/L Tris-HCl (pH 6.8), 100 mmol/L DTT, 2% SDS, 0.1% bromophenol blue, 10% glycerol] and then boiled for 10 min. Standard Western blotting analyses were performed. Lysates in DTT-containing SDS sample buffer were separated in 8% or 12% SDS-polyacrylamide gels and transferred to PVDF transfer membranes (Thermo) and incubated with primary antibodies including anti-HIF1 α , anti-PPAR δ , and anti-GAPDH (antibodies diluted

concentration following the manufacturer's instructions). Expression was then detected with BioRad ChemDoc MP Imaging System using blotting-grade HRP conjugate (Bio-rad) and Immobilon Western Chemiluminescent HRP Substrate (Millipore) for chemiluminescent detection. All antibodies are listed in **Table S2**.

Luciferase reporter assay

5×10^4 per well of HEK293T cells were seeded in 24 well plates and transfected with plasmids of 250 ng HRE-Luc, 25 ng pRL-CMV Renilla (Rluc) and with or without 250 ng Flag-PPAR δ . Luciferase activity was measured after 24 h by dual luciferase assay following the manufacturer's instructions (Promega, USA). The relative luciferase activity was determined by firefly luciferase value versus renilla luciferase value. The presented data showed the fold change normalized to control group.

HIF1 α half-life assays

The BMECs were exposed to hypoxia (1% O₂) for 4 h after transfected with *Ppard* siRNA for 48 h. Cells were exposed to 50 μ g/mL cycloheximide (Sigma, cat#01810) for the indicated time to block protein synthesis. The cells were collected for Western blotting.

Chromatin Immunoprecipitation analysis (ChIP)

ChIP assay was carried out according to the previously published method [29]. Briefly, Hela cells were lysed in ChIP-IP buffer (150 mmol/L NaCl, 50 mmol/L Tris-HCl (pH 7.5), 5 mmol/L EDTA, NP-40 (0.5% vol/vol), Triton X-100 (1.0% vol/vol)) with addition of protein inhibitors (Sigma, cOmplete™ Protease Inhibitor Cocktail). After sonication, centrifugation and protein A/G agarose beads pretreatment (Pierce™ Protein A/G Agarose, #20421), clear supernatant was incubated with anti-HIF1 α primary antibody for 6 h and then immunoprecipitates were captured by protein A/G agarose beads for another 4 h incubation. Finally, the chromatin DNA was eluted in 10% (wt/vol) Chelex 100 slurry ((Bio-Rad, #142-1253) by boiling for 10 min.

Immunoprecipitation

Cell lysates were prepared in IP lysis buffer (20 mmol/L Tris-HCl (pH 7.9), 200 mmol/L NaCl, 5 mmol/L MgCl₂, 10% glycerol, 0.2 mmol/L EDTA, and 0.1% NP-40) supplemented with protease and phosphatase inhibitors (Sigma, complete™ Protease Inhibitor Cocktail and PhosSTOP™). Clear cell supernatant was incubated with the respective anti-Flag or HA agarose beads for 4 h at 4 °C. After the beads were washed with IP lysis buffer three times,

the immunoprecipitates were eluted in Laemmli sample buffer and subjected to western blotting analysis.

Evans blue staining

After HLI at day 10, mice were injected with 300 μ L of 1% Evans Blue (in PBS) via the tail vein. The dye was allowed to circulate in vivo for 30 min, followed by cardiac perfusion with PBS (10 mL per mouse). Quadriceps were isolated and weighed, and the dye was extracted overnight with deionized formamide (1 mL per muscle) and measured at an optical density of 610 nm.

FITC dextran extravasation

After HLI at day 7, mice were injected with 50 μ L 25 mg/mL 70 kDa FITC dextran (Sigma, cat# FD70S) via the tail vein 30 min before sacrifice. Microscopic visualization of FITC dextran extravasation was performed on OCT-embedded tissue sections and co-stained with anti-CD144 antibody (Invitrogen).

Adeno-associated viruses (AAV) administration

For AAV-mediated *Icam2*-driving *HIF1A*-P402A/P564A (M1 in short) or *HIF1A*-(Δ ODD)/R27G (ODD domain deleted, M2 in short) overexpression, the M1 and M2 viruses (total 10^{11} vg in 30 μ L was injected into the hindlimb muscles of both sides 1 week before HLI.

Statistical analysis

All data were presented as means \pm SEM and the numbers of independent experiments are indicated. Flow cytometry data were analyzed by FlowJo. Western blot images were analyzed by ImageJ. Student's t test was used for comparison between two samples, and one-way ANOVA and multiple comparison test was used for more than two samples in GraphPad Prism. * $p < 0.05$, ** $p < 0.01$, and *** $p < 0.001$ was indicated as statistically significant.

Results

Selective deletion of endothelial *Ppard* impairs vascular perfusion in mice after hindlimb ischemia

After generating the endothelial selective *Ppard* knockout *Ppard*^{EC-KO} and wild type *Ppard*^{EC-WT} mice, the knockout efficiency was tested in endothelial cells (ECs) from several organs showed diminished *Ppard* mRNA expression and protein expression (Figure S1A, B). Vascular perfusion measurement after hindlimb ischemia (HLI) showed that recovery of perfusion was reduced in the *Ppard*^{EC-KO} mice over a

period of 3 weeks (Figure 1A-B). Similar results were also obtained by imaging of vascular structure at 7 days after HLI (Figure 1C-D). At the end of 3 weeks, toenail necrosis as one of the parameters of ischemic score [30], could still be observed in the *Ppard*^{EC-KO} mice, reflecting an impaired recovery (Figure S1C-D). The gastrocnemius (GA) muscle became smaller after HLI which was further reduced in the *Ppard*^{EC-KO} mice (Figure 1E), with less regenerating muscle fiber with centralized nuclei, and more scar formation replacing muscle fiber in the GA of *Ppard*^{EC-KO} mice (Figure 1F-H). Delayed muscle repair in the *Ppard*^{EC-KO} mice was also observed from the gene profiling which showed the delayed upregulation of muscle progenitor markers *Pax3* and *Pax7*; early myogenic markers *Myf5*, *Myod1*, and *Myog*, shifting from normally 3 and 7 days to a later time point at 14 days (Figure 1I). In addition, the endothelium-dependent vasodilatation induced by acetylcholine (Figure 1J) was impaired after HLI in the femoral arteries from *Ppard*^{EC-KO} mice, indicating sustained impairment of endothelial function; whereas nitric oxide (NO) donor sodium nitroprusside (SNP) induced vasodilatation was similar, indicating the smooth muscle function was less affected (Figure S1E). These results suggested a delayed structural and functional recovery after HLI due to loss of endothelial PPAR δ .

Deletion of endothelial *Ppard* impairs post-ischemic angiogenesis

Because PPAR δ ligands stimulate angiogenesis in endothelial cells [17-20], although the endothelial deletion of *Ppard* was not fully characterized, we first examined whether post-ischemic angiogenesis was affected by EC selective deletion of PPAR δ . Immunofluorescence showed that the post-ischemic increase of VEGFR2, as well as CD31, was less in the *Ppard*^{EC-KO} mice (Figure 2A). Expression of α -SMA showing the arterioles also increased less in the *Ppard*^{EC-KO} mice (Figure 2A). Notably, FITC-lectin which labels the functional endothelium showed diminished signals in the *Ppard*^{EC-KO} mice (Figure 2A-B). Flow cytometric analysis demonstrated less increase of EC labeled as CD45-CD31⁺ cells in *Ppard*^{EC-KO} mice (Figure 2C-D). Similarly, qPCR analysis of mRNA expression suggested several angiogenic factors such as *Vegfa*, *Fgf2*, did not increase similar as wild type after ischemia, while the induction of some angiogenic factors such as *Angpt1* and *Tie2* were delayed (Figure 2E). In vitro, the aortic segments from the *Ppard*^{EC-KO} mice also showed less sprouting (Figure S2A-B). These results suggested impaired post-ischemic hypoxia-induced angiogenesis due to the loss of PPAR δ in ECs.

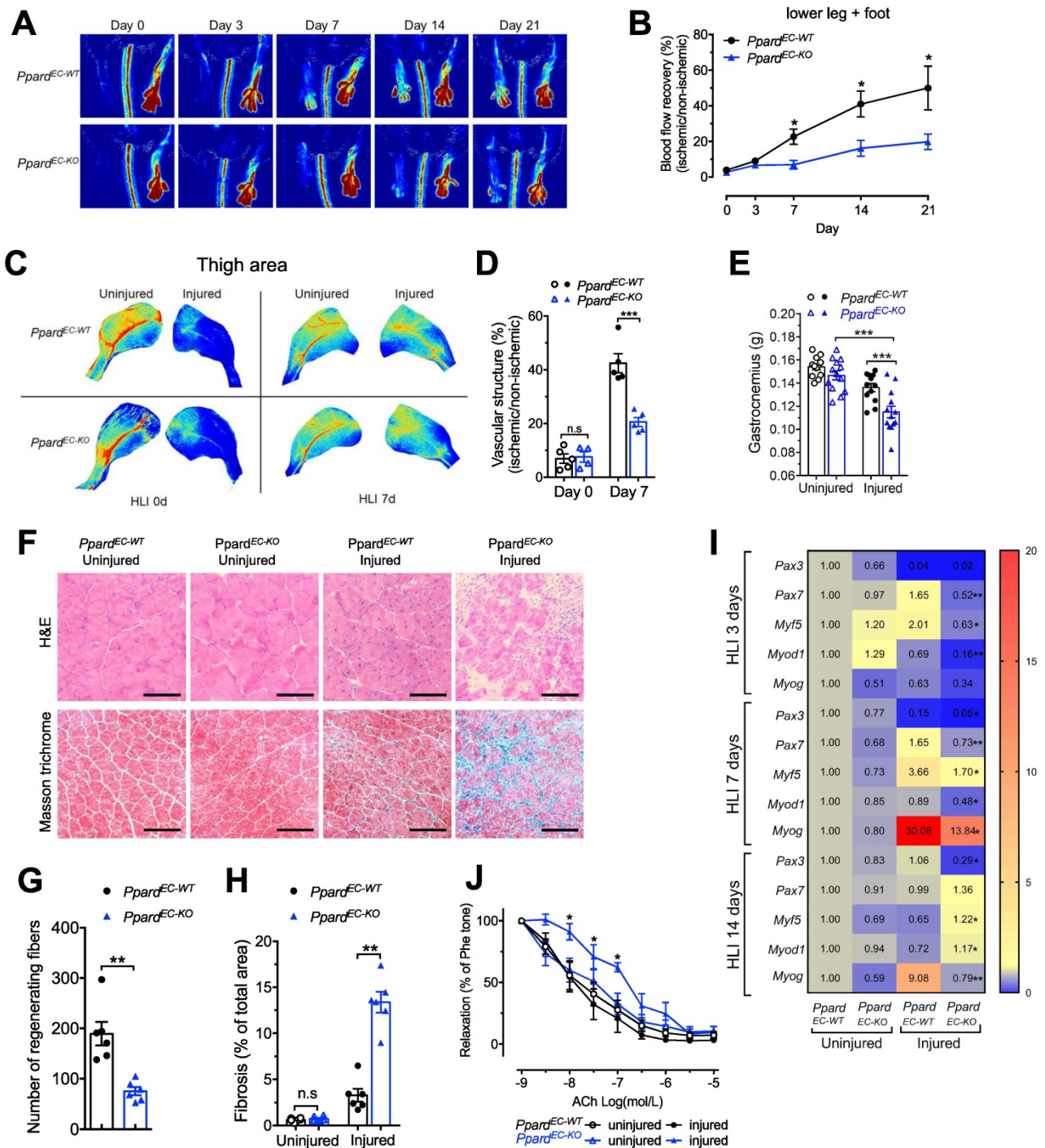


Figure 1: Endothelial deletion of *Ppard* impairs vascular remodelling and damages skeletal muscle regeneration. Perfusion imaging following HLI, showed in representative images (A) and analysis in (B) (n = 6 mice for each group). C-D, Representative images of Vasculature imaging in leg area were recorded at days 0 and 7 in representative images (C) and summarized analysis in (D) (n = 5, each group). E, Muscle weights of gastrocnemius (GA) were measured at days 14 after HLI. F, Haematoxylin/eosin staining (up) and Masson trichrome staining (bottom) at days 14 after HLI (n = 6, each group). Scale bar, 100 μm. G, Quantification of regenerating muscle fibers based on H&E staining. H, Quantification of fibrosis (blue colour) based on trichrome staining. I, Heatmap of qPCR data at days 3, 7, 14 after HLI. The number in each cell represents the fold change compared with *Ppard*^{EC-WT} uninjured GA (n = 5-6, each group). Results are means ± SEM. J, Concentration-response curves to acetylcholine (ACh) in femoral arteries at days 28 after HLI. Results are means ± SEM. * p < 0.05, ** p < 0.01, *** p < 0.001 between groups or vs injured *Ppard*^{EC-WT}. Student's t test was used for comparison between two samples, and one-way ANOVA and multiple comparison test was used for more than two samples.

Deletion of endothelial *Ppard* exacerbates vascular hyperpermeability

Endothelial barrier function is an important aspect indicating the functional restoration of injured vasculature [31]. Whether endothelial barrier function

is regulated by PPARδ is unknown. To examine vascular barrier integrity, we first showed that a lot more albumin leakage surrounding the capillaries after HLI was found in the *Ppard*^{EC-KO} mice, which is a parameter to assess vascular hyperpermeability

(Figure S3). This change was also quantified by Evans blue, a dye binding to serum albumin which also showed more leakage into the injured muscles from *Ppard*^{EC-KO} mice (Figure 3A-B). We then used FITC labelled 70-kDa dextran administration to examine the EC junctional alterations, in which the aggregated FITC at capillaries indicates increased extravasation in the injured muscles from *Ppard*^{EC-KO} mice which was persistent after HLI (Figure 3C). Two junctional proteins CD144 and tight junction ZO-1, which are functionally important in ECs, also became more discontinuous in the newly emerged capillaries of *Ppard*^{EC-KO} mice (Figure 3D, indicated by yellow arrowheads), which was more continuous in the capillaries from *Ppard*^{EC-WT} mice (Figure 3D, indicated by white triangles). In addition, the upregulation of several genes including *Cldn5*, *Tjp1* (ZO-1), *Ocln* (occludin), which are involved in tight junction (Figure 3E-G); as well as *Nectin1*, *F11r* (Jam-A), and *Jam2* (Jam-b) which are involved in adherens junction and endothelial leukocyte adhesion (Figure 3H-J), were attenuated in the injured muscle from *Ppard*^{EC-KO} mice. These results indicated impaired restoration of endothelial barrier function due to the loss of PPAR δ

after HLI.

Deletion of endothelial *Ppard* promotes endothelial activation and inflammatory responses

Because impaired endothelial integrity promotes endothelial activation, we characterized vascular inflammatory responses after HLI. Immuno fluorescence showed that macrophage and T lymphocyte infiltrations were increased in the ischemic muscle from *Ppard*^{EC-KO} mice (Figure 4A). More accumulation of tissue macrophages (labeled as F4/80⁺Ly6C^{lo}), which was likely due to the infiltration of monocyte-derived macrophages (F4/80^{mid}Ly6C^{hi}) was also observe by flow cytometric analysis (Figure 4B-C). Consistently, many vascular inflammatory factors including adhesion molecules *Icam1*, *Vcam1* and *Sele* (*E-selectin*) (Figure 4D-F), chemokine and their receptors *Ccr2*, *Ccl2*, *Cx3Cr1* (Figure 4G-I), and cytokine *Il1b* and *Il-6* (Figure 4J-K), also remained at high level in the ischemic muscle from *Ppard*^{EC-KO} mice. These results indicated that loss of PPAR δ in ECs caused a persistent endothelial activation and unresolved chronic inflammation after HLI.

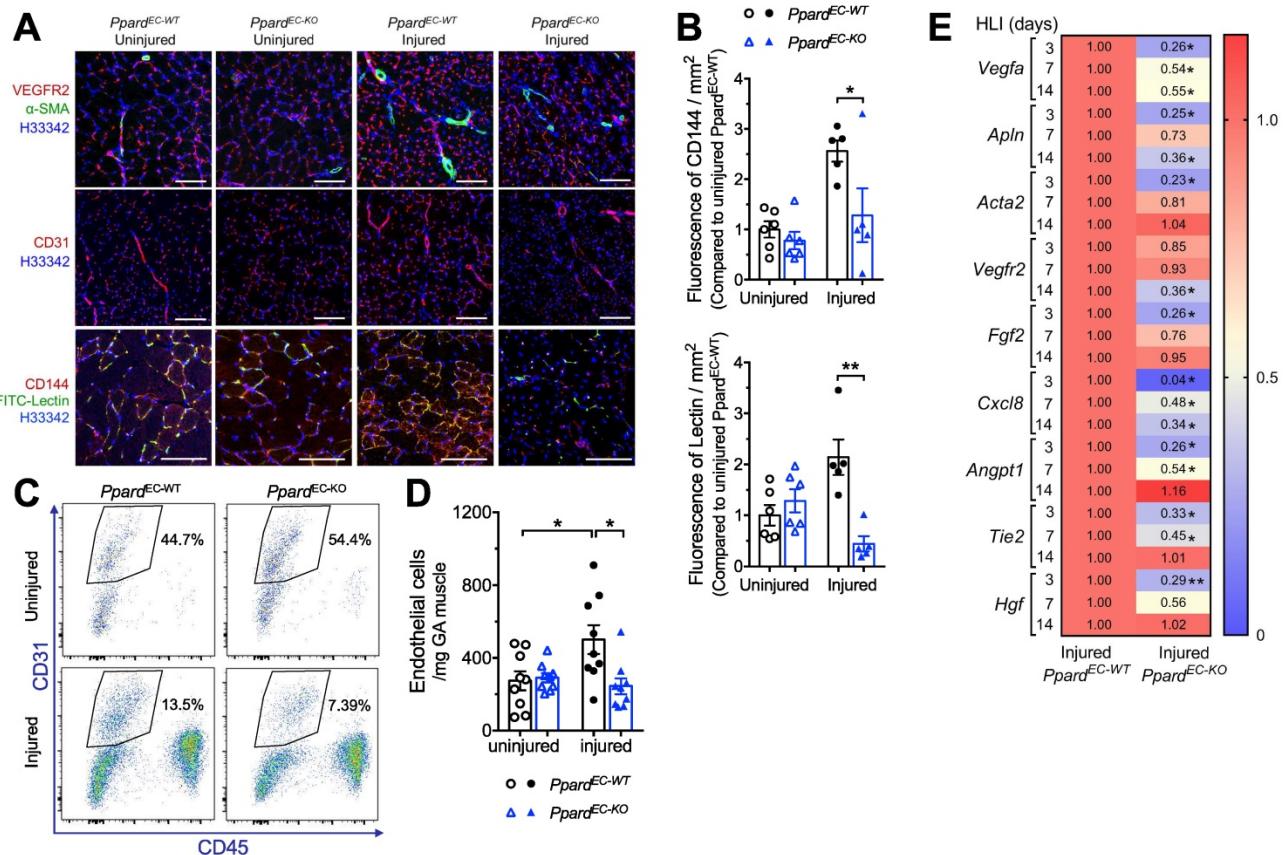


Figure 2: Deletion of endothelial *Ppard* impairs post-ischemic angiogenesis. **A**, Muscle frozen sections stained with VEGFR2, CD31 and CD144 for ECs, α -SMA for arteriole and FITC-lectin for functional vessel (n = 6, each group). Scale bar: 200 μ m. **B**, Analysis of FITC-lectin to identify functional microvessels and CD144 to identify ECs at days 14 after HLI (n = 6, each group) for **Figure 3A**. **C** (representative flow plots) and **D** (summarized analysis) of CD45-CD31⁺ ECs at day 3 after HLI. **E**, Heatmap of the qPCR data for angiogenesis related genes at indicated time after HLI. The number in each cell represents the fold change compared with *Ppard*^{EC-WT} injured GA (n = 5-6, each group). Results are means \pm SEM. * p < 0.05, ** p < 0.01 between groups. Student's t test was used for two samples, and one-way ANOVA and multiple comparison test was used for more than two samples.

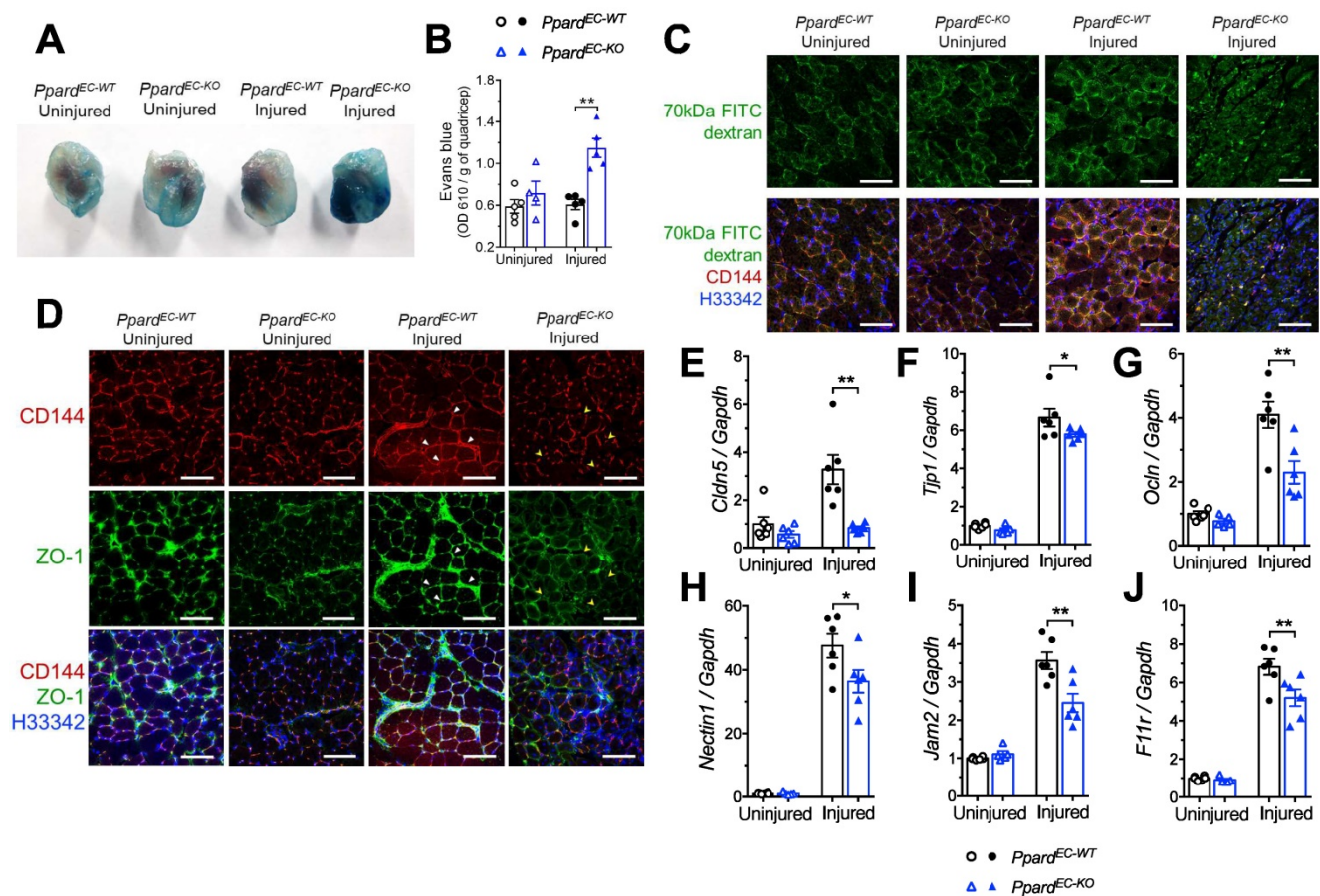


Figure 3: Deletion of endothelial *Ppard* increases vascular permeability. **A** (Representative images) and **B** (quantification) of Evans Blue in quadriceps 14 days after HLI. **C**, Representative images of FITC-labeled 70 kDa dextran co-stained with CD144 in GA at day 7 after HLI (n = 5, each group). Scale bar: 200 μ m. **D**, Representative images of ZO-1 to co-localize with CD144 in GA at day 10 after HLI (n = 6, each group). Scale bar: 200 μ m. Triangle indicates continuous endothelium. Arrowhead indicates discontinuous endothelium. **E–J**, qPCR analysis of muscles 3 days after HLI (n = 6, each group). Results are means \pm SEM. * p < 0.05, ** p < 0.01 between groups by one-way ANOVA and multiple comparison test.

PPAR δ enhances HIF1 α activity in endothelial cells in response to hypoxia

During ischemic injury, endothelium is exposed to hypoxia. To examine the response of ECs to hypoxia, we first used bone marrow –derived endothelial progenitor cells (EPCs) which are capable of angiogenesis in vitro, rather than using primary ECs from muscle due to the difficulty of maintaining primary EC phenotype in vitro. We observed that tube formation enhanced by hypoxia was impaired in *Ppard*^{EC-KO} EPCs (Figure 5A, analysis in Figure S4A–D). In response to hypoxia, hypoxia-inducible factor (HIF1 α) is activated and induces downstream gene expression for vascular regeneration and remodeling in endothelial cells [32]. Therefore, we wondered whether PPAR δ might modulate HIF1 α activity in regulating EC function. Hypoxia upregulated PPAR δ mRNA (Figure 5B) and protein (Figure 5C) expression in BMECs. Meanwhile, *Ppard* siRNA treatment attenuated hypoxia-induced upregulation of HIF1 α protein in BMECs (Figure 5C). However, HIF1 α mRNA expression was not affected

by *Ppard* siRNA (Figure S4E). In addition, we observed the hypoxia-induced upregulation of several well-known HIF1 α target genes such as *Vegfa*, *Vegfr2*, *Pdk1*, as well as *Angptl4*, the common target gene of both PPAR δ and HIF1 α , were attenuated by silencing of *Ppard* in BMECs (Figure S4F–I). We then asked whether PPAR δ might be directly involved in HIF1 α -mediated transactivation. As expected, co-expression of PPAR δ with HIF1 α enhanced the hypoxia responsive element (HRE) -driven luciferase activity, whereas PPAR δ alone had minimal effect (Figure 5D). Furthermore, ChIP assay showed that there was less HIF1 α occupancy at the HRE region of *GLUT1*, a well-characterized HIF1 α target gene [33], after silencing of *PPARD* in HeLa cells (Figure S4J–K). These results suggested that PPAR δ underlines HIF1 α transactivation.

We thus asked how PPAR δ regulated HIF1 α transactivation. Because *HIF1A* mRNA was unaffected by *Ppard* siRNA, we asked whether PPAR δ regulates HIF1 α protein stability. First, we performed cycloheximide (CHX) chase assay and found a significant decline in HIF1 α protein stability

in the BMECs after silencing *Ppard* (Figure 5E). Conversely, overexpressing PPAR δ stabilized ectopic HIF1 α (Figure 5F). Because HIF1 α protein degradation is largely dependent on the ubiquitin-proteasome system [34], proteasome inhibitor MG132 was sufficient to restore HIF1 α protein in the presence of CHX (Figure 5F). We therefore wondered whether PPAR δ modulates HIF1 α ubiquitination. As determined by *in vivo* ubiquitination assay, ubiquitinated HIF1 α declined notably with PPAR δ overexpression (Figure 5G). Together, these results suggested that PPAR δ stabilizes HIF1 α via inhibiting ubiquitination dependent proteasome-mediated degradation.

PPAR δ interacts with HIF1 α in endothelial cells

We reasoned that PPAR δ was less likely to act on HIF1 α by directly writing or erasing any post-translational modifications of HIF1 α protein. Because previous study showed that HIF1 α could be

stabilized by forming complex with co-factors, such as c-Jun, to mask the oxygen dependent degradation (ODD) domain, preventing HIF1 α from ubiquitination-dependent degradation [35], we wondered whether PPAR δ acts through a similar mechanism. Firstly, co-immunoprecipitation showed that HA-HIF1 α or HA-PPAR δ existed in the immunoprecipitate of anti-Flag-PPAR δ or anti-Flag-HIF1 α (Figure 6A), suggesting the interaction between PPAR δ and HIF1 α . Next, PPAR δ failed to bind with ODD-deleted HIF1 α , indicating that PPAR δ directly occupies the ODD domain of HIF1 α to prevent its degradation (Figure 6B). In addition, PPAR δ enhanced the formation of HIF1 α / β heterodimer (Figure 6C), which is crucial to for HIF1 α transactivation. However, the direct interaction of HIF1 β with PPAR δ was nearly undetectable (Figure S5A). Collectively, our results suggested that PPAR δ acts as a co-factor stabilizing HIF1 α transcriptional complexes.

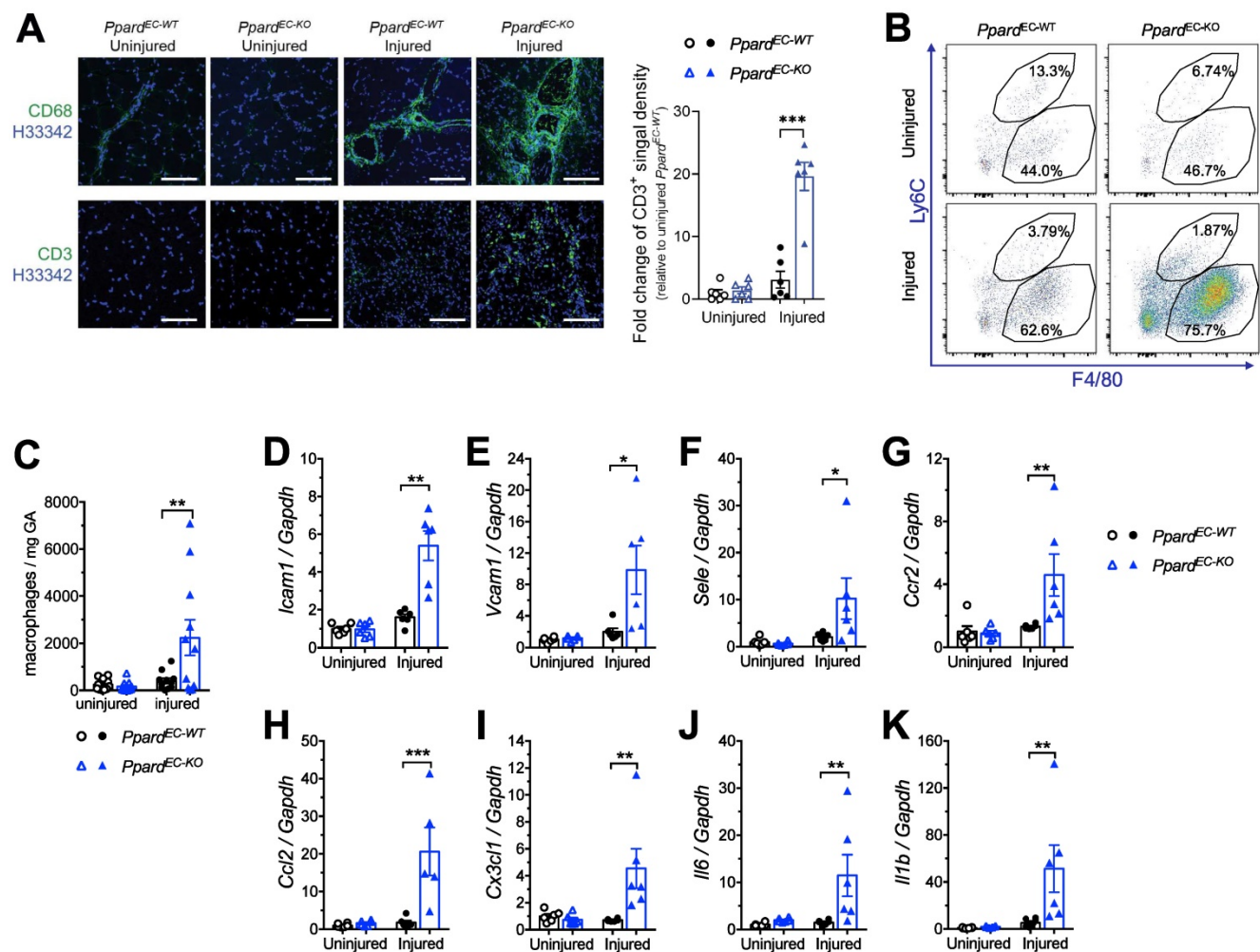


Figure 4: Deletion of endothelial *Ppard* enhances endothelial activation and inflammatory responses. **A**, Representative images of immunofluorescence showing CD68 staining (upper) and CD3 (lower) 14 days after HLI (n = 5, each group). Scale bar: 200 μ m. **B** (Representative flow plots) and **C** (summarized analysis) of F4/80^{hi}Ly6C^{hi} monocyte/macrophages and F4/80⁺Ly6C^{low} macrophages at day 10 after HLI. **D-K**, qPCR analysis for vascular inflammatory markers Vcam1, Icam1 and E-selectin in GA 14 days after HLI (n = 6, each group). Results are means \pm SEM. * p < 0.05, ** p < 0.01 between groups by one-way ANOVA and multiple comparison test.

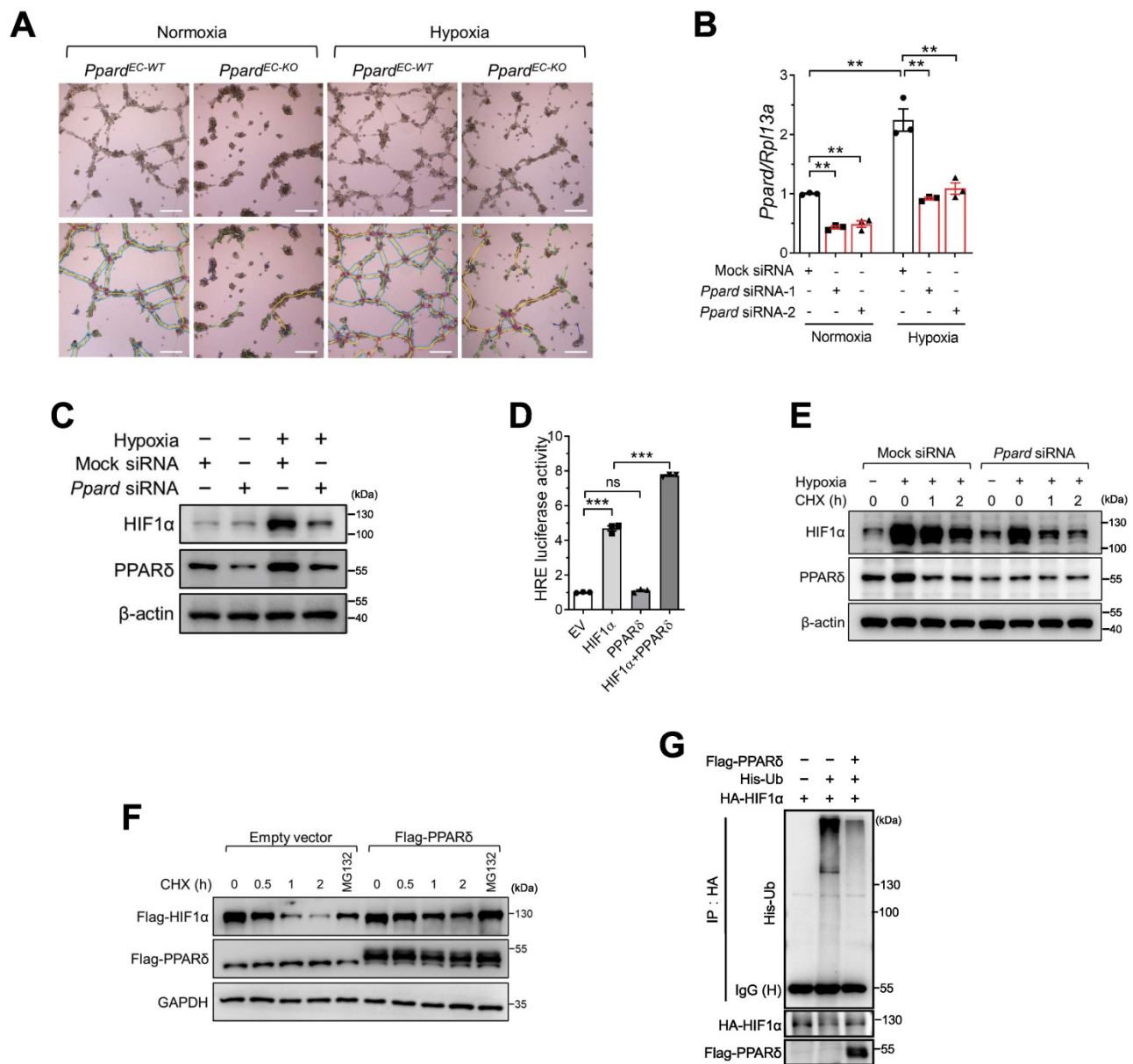


Figure 5: PPARδ enhances HIF1α activity in endothelial cells in response to hypoxia. **A** (representative images) and **B** (summarized analysis) of tube formation of bone marrow-derived endothelial cells on matrigel under normoxia and hypoxia, analyzed using the Angiogenesis Analyzer of Image J (n = 4, each group). Scale bar: 100 μm. **C**, Immunoblots showing HIF1α treated with *Ppard* siRNA in mBMECs under hypoxia for 12h. **D**, Luciferase reporter assay showing HRE-luc activity in HEK293T cells transfected with indicated plasmids. EV: empty vector. **E**, Immunoblots showing the effect of CHX 50 μg/mL at indicated time after hypoxia for 4 h. **F**, Immunoblots in HEK293T following indicated treatments under normoxia. CHX, 50 μg/mL. MG132, 10 μmol/L. **G**, In vivo ubiquitination assay showing the ubiquitinated HIF1α levels in HEK293T after transfection of indicated plasmids. Representative data have at least three biological replicates. Results are means ± SEM. * p < 0.05, ** p < 0.01 between groups by one-way ANOVA and multiple comparison test.

Hypoxia induces ligand-independent activation of PPARδ

PPARδ has an N-terminal DNA-binding domain (DBD) and a C-terminal ligand-binding domain (LBD) for ligand-induced transactivation [28]. We further investigated which domain was required for HIF1α binding. As shown by co-IP, HIF1α had a strong affinity to both full-length, and LBD, but not DBD, suggesting LBD underlies the recruitment of HIF1α (Figure 6D). We thus wonder whether the interaction of HIF1α and PPARδ relies on its ligand. Interestingly,

PPARδ agonist GW501516 does-dependently counteracted the binding of HIF1α to PPARδ (Figure 6E), indicating that the interaction between HIF1α and PPARδ under hypoxia was most likely independent of PPARδ ligand. GW501516 did not increase HIF1α protein (Figure S5B) or its target genes such as *Vegfa* under hypoxia in BMECs (Figure S5C-D), whereas PPARδ target gene *Pdk4* was induced by GW501516, and also enhanced by hypoxia (Figure S5E). In addition, GW501516 did not increase hypoxia-induced PPARδ upregulation (Figure S5F). Taken together, these results suggested that PPARδ

enhanced HIF1 α target gene expression most likely relied on PPAR δ protein upregulation but not ligand driving activation.

Hypoxia also upregulated PPAR δ in BMECs at both protein and mRNA level (Figure 5B-C, Figure 6F), which was attenuated at protein level by *Hif1a* siRNA in BMECs (Figure 6F) and also at mRNA level in Hela cells (Figure S4K), indicating that HIF1 α might be able to regulate PPAR δ transcription. In additional,

hypoxia also induced more PPAR δ translocation to the nuclei as shown by immunofluorescence in BMECs (Figure 6G), implying that under hypoxia, not only PPAR δ expression is increased, but it is also more accessible to interact with HIF1 α . Altogether, our results indicated that hypoxia upregulates PPAR δ expression by HIF1 α and PPAR δ reciprocally stabilizes HIF1 α protein which could be responsible for post-ischemic vascular repair.

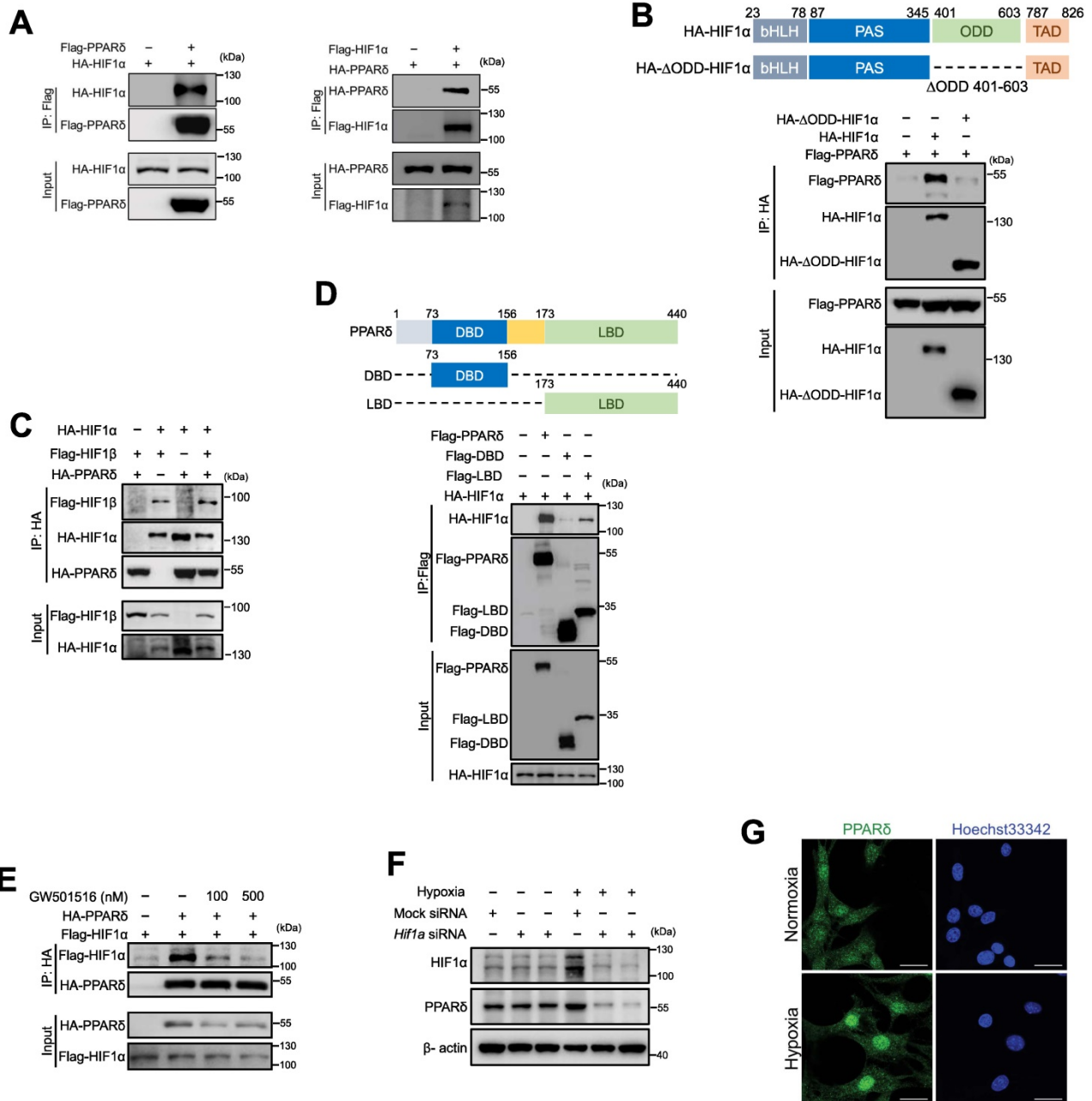


Figure 6: Hypoxia-induced PPAR δ interacts with HIF1 α in endothelial cells. **A**, Immunoblots showing HIF1 α and PPAR δ in anti-Flag immunoprecipitates in HEK293T transfected with indicated plasmids. **B**, Schematic diagram showing site of Δ ODD in HIF1 α gene and immunoblots showing the Flag-PPAR δ in the anti-HA immunoprecipitates from cells co-expressing Flag-PPAR δ and full-length HA-HIF1 α or Flag-PPAR δ and ODD domain deleted HIF1 α (HA- Δ ODD-HIF1 α). **C**, Immunoblots showing the anti-HA immunoprecipitates in HEK293T with transfection of indicated plasmids. **D**, Schematic diagram showing the position of full-length and truncated PPAR δ DBD and LBD, and immunoblots showing the anti-Flag immunoprecipitates in HEK293T with indicated plasmids transfected. **E**, Immunoblots showing the anti-HA or anti-Flag immunoprecipitates in HEK293T with indicated plasmids transfected to show the interaction of PPAR δ and HIF1 α treated with GW501516 (6 h) or solvent control. **F**, Immunoblots of protein expression after transfection with *Hif1a* siRNA in mBMECs after hypoxia for 12 h. **G**, Representative immunofluorescence of PPAR δ localization in the nuclei of mBMECs after hypoxia for 12 h (n = 4 biological replicates of each group). Scale bar, 20 μ m. All the siRNA transfections were performed with lipofectamine RNA iMax for 48 h, and all the plasmids were transfected with lipofectamine for 36 h, before other treatments. Representative data have at least three biological replicates (**A-F**).

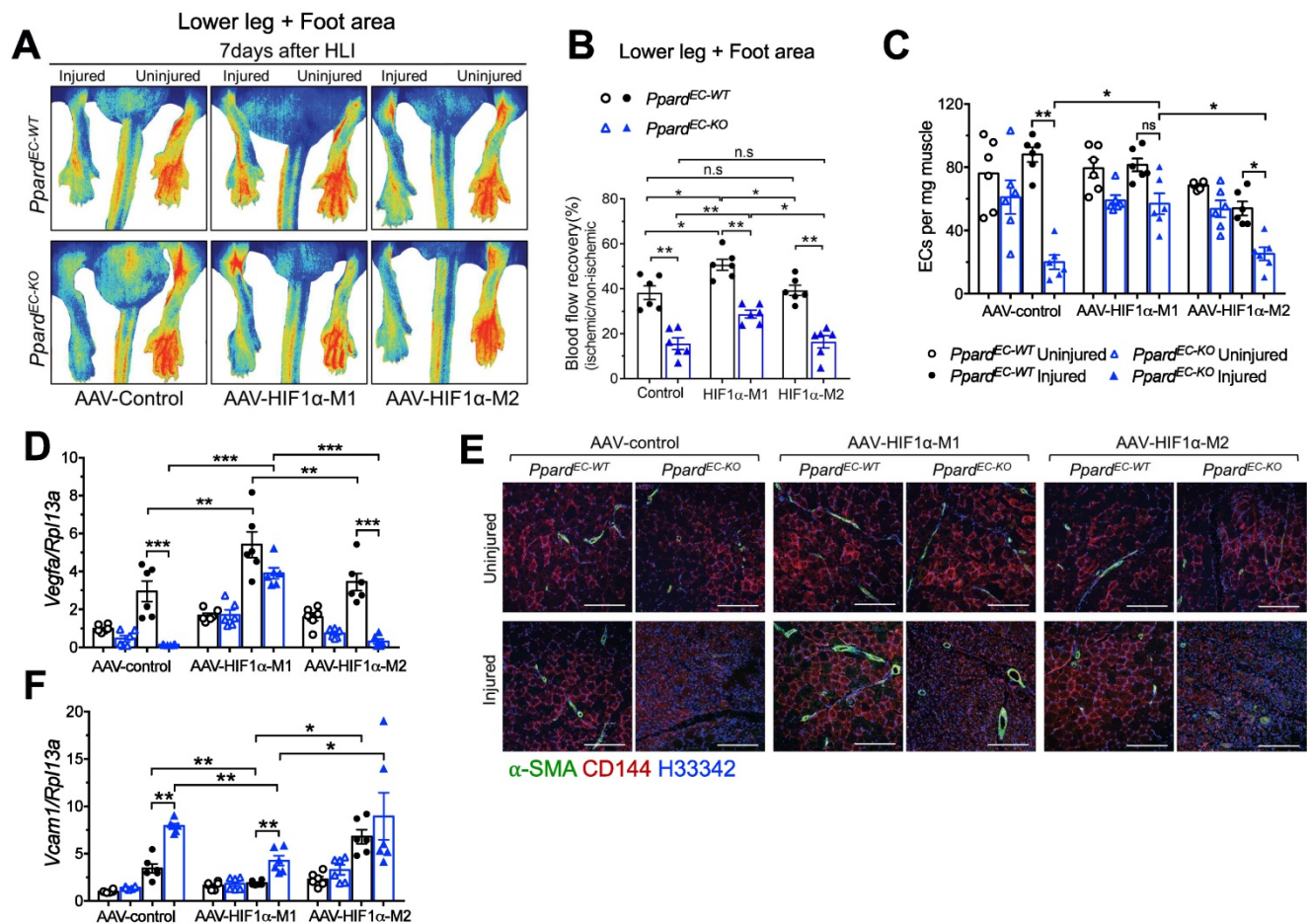


Figure 7: Expression of stable HIF1 α in endothelial cells improves vascular repair. **A** (representative images) and **B** (summarized analysis) showing vasculature imaging in mouse foot area recorded at day 7 after HLI (n = 6, each group). **C**, flow cytometric analysis of CD45⁺CD144⁺ECs at day 7 after HLI (n = 6, each group). **D&F**, qPCR analysis for Vegfa (**D**) and Vcam1 (**F**) mRNA expression in muscles collected 7 days after HLI (n = 6, each group). **E**, Representative immunofluorescence of α -SMA co-stained with CD144 in muscle at day 7 after HLI (n = 6, each group). Scale bar: 200 μ m. Results are means \pm SEM. * p < 0.05, ** p < 0.01, between groups by one-way ANOVA and multiple comparison test.

Expression of stable HIF1 α improves the delayed vascular repair due to loss of endothelial PPAR δ

Because in vitro experiments indicated a strong interaction between PPAR δ and HIF1 α , we further studied whether stable HIF1 α would rescue the delayed vascular repair induced by loss of endothelial PPAR δ . To do it, we used AAV to overexpress either the stable and active M1-HIF1 α which has P402A/P564A mutation allowing HIF1 α to maintain stabilization by preventing its hydroxylation and binding to E3 ubiquitin ligase [36], or the negative control M2-HIF1 α (HIF1 α (Δ ODD)/R27G), in which the ODD domain was removed. This ODD modification makes HIF1 α stable at normoxia but R27G mutation further abolishes the DNA binding ability, which makes the M2-HIF1 α stable but lacking transcriptional activity [25]. AAV to overexpress M1 or M2 selectively in ECs driven by *Icam2* promoter was injected one week before HLI. Expression of HIF1 α from both M1 and M2 could be detected in

CD144⁺ ECs (Figure S6A). Expression of HIF1 α target genes *Pdk1*, *Adm*, and *Glut1* after HLI was increased more in the muscles from M1 than M2 (Figure S6B-D). Vascular perfusion was enhanced in *Ppard*^{EC-KO} by HIF1 α -M1, although the perfusion in *Ppard*^{EC-KO} with HIF1 α -M1 was still worse than *Ppard*^{EC-WT}, suggesting both HIF1 α -dependent and -independent effects regulated by PPAR δ (Figure 7A-B). Meanwhile, the effect of HIF1 α -M2 was similar to AAV-control. EC numbers as an indicator of post-ischemic angiogenesis were quantified by flow cytometric analysis which showed that HIF1 α -M1 but not M2 increased EC number in *Ppard*^{EC-KO} mice at 7 days post-HLI (Figure 7C). Consistently, Vegfa expression was also higher with M1 (Figure 7D). In addition, CD144 and α -SMA upregulations were observed in both *Ppard*^{EC-KO} and *Ppard*^{EC-WT} mice after HIF1 α -M1 but not M2 injection (Figure 7E). Importantly, CD144 expression in HIF1 α -M1, but not control or M2, was less discontinuous (Figure 7E), indicating better repair of a functional endothelium induced by HIF1 α -M1. Likewise, upregulation of Vcam1 was attenuated by

HIF1 α -M1, whereas M2 remained similar as control (Figure 7F). These results suggested that restoring HIF1 α expression and activity improved the vascular

Discussion

In this study, we investigated endothelial selective loss of PPAR δ expression in ischemic injury. We found that PPAR δ orchestrates many functional aspects of ECs including angiogenesis, vascular reactivity, vascular barrier function, and inflammatory responses, associated with HIF1 α signaling. We also found that hypoxia upregulates PPAR δ , which interacts and stabilizes HIF1 α , during which the two transcription factors enhance the expression and transactivation of each other.

Although several previous studies showed the effect of PPAR δ in ECs and other vascular cells, many were based on the effect of ligands, with little known about how PPAR δ responds and changes to vascular injury. The effect of PPAR δ on angiogenesis was mostly only observed in isolated ECs using pharmacological ligands. PPAR δ ligands including L-165041, GW501516, and prostacyclin [37], enhance angiogenesis and prevent apoptosis in human EPCs [18, 21]. These human EPCs, when injected into mice, showed impaired angiogenesis with silencing of PPAR δ [21]. PPAR δ ligands also enhance angiogenesis by regulating GTPCHI and BH $_4$ related to eNOS activity [19], as well as upregulation of angiogenic factors like VEGFs [37]. However, the influence of *in vivo* loss of PPAR δ on angiogenesis or other functions of EC, in addition to vascular tone, remains unclear. The involvement of endogenous PPAR δ has only been shown recently using global *Ppard* knockout mice which suggested a reduced retinal angiogenesis and vessel remodeling only at steady state [38]. In the present study, we found that ischemia-induced angiogenesis and possibly vasculogenesis was impaired in the *Ppard*^{EC-KO} mice, suggested by a delayed appearance of capillary ECs and arterioles, accompanied by the failure to upregulate many angiogenic factors including the VEGF signaling.

In addition to regeneration of vasculature, restoration of endothelial barrier function is also important for recovery of microvessel function in PAD. Previous studies on PPAR δ mostly focused on other vasculatures excluding the muscle capillaries. GW0742 help to reduce blood brain barrier leakage after brain injury [39]. However, opposite effect was observed in retinal ECs, using *PPARD* siRNA and inhibitor to reduce VEGF-induced hyperpermeability [40]. We speculate that the opposite effect might be due to the different responses of PPAR δ under different oxygen tension, and therefore, might be

repair impaired by endothelial *Ppard* deletion, while some effects of PPAR δ might be HIF1 α -independent.

influenced by HIF1 α . Furthermore, delayed recovery of barrier function from both the existing and newly regenerated ECs in the *Ppard*^{EC-KO} mice might lead to more persistent endothelial activation and vascular inflammation after HLI. Although PPAR δ ligands have been known for its potent anti-inflammatory effects, we showed here a previously unrecognized contribution of endogenous PPAR δ against vascular inflammation in response to ischemic injury. All these results suggested an important role of PPAR δ in restoring vascular homeostasis after ischemic injury. The vascular phenotype of *Ppard*^{EC-KO} mice was also under-explored. Using a different strain of endothelial Cre, the Tie2-Cre to generate endothelial selective *Ppard* knockout mice (*Ppard*^{flxed};Tie^{Cre/+} mice), another group showed a small but significant impairment of endothelium-dependent relaxation in the aorta in response to ACh under unstimulated condition due to increased H $_2$ O $_2$ production which decreased NO availability [41]. Such differences might be due to sensitivity of ligand and to NO in femoral arteries different from aorta, and also possibly due to strain differences.

To provide a more mechanistic role of how endothelial PPAR δ regulates vascular homeostasis, we further studied the role of HIF1 α . The present results suggested that endogenous PPAR δ could be activated in response to hypoxic stress. Notably, PPAR δ regulates HIF1 α protein by reducing HIF1 α degradation in ECs under hypoxia. Such effect was likely due to the interaction between the LBD domain of PPAR δ and the ODD domain of HIF1 α . To further confirm the regulation of HIF1 α by PPAR δ *in vivo*, we used AAV to overexpress stable HIF1 α which was able to ameliorate the delayed vascular repair due to loss of PPAR δ . Interestingly, this mechanism of ligand-independent regulation of HIF1 α by PPAR δ from our study is different from a previous study which showed overlapping of transcriptome regulation in PPAR δ agonist -treated and hypoxia-treated human ECs [42]. Future study to assess the effect of PPAR δ ligand on angiogenesis in the *Ppard*^{EC-KO} mice, which might strengthen the current finding. It is also unclear whether and which endogenous ligand(s) is playing a major role in the activation of PPAR δ after HLI. Nevertheless, these results suggested a ligand-independent role of PPAR δ to respond to hypoxia and to facilitate the restoration of vascular homeostasis through enhancing HIF1 α function.

The role of HIF1 α in post-ischemic vascular responses has been well established by studies using

either gain- or loss-of-function [43, 44]. Apart from angiogenesis, HIF1 α also regulates other functions of ECs such as stimulating proliferation, inhibiting microvascular leakage and enhances vascular repair [45]. Several proteins such as NQO1, Runx2 [46] and CBX4 [47], etc., have been identified to interact with the ODD domain of HIF1 α , and as a result, enhances HIF1 α stability and HIF1 α -mediated angiogenesis. Here we showed a new role of PPAR δ to stabilize HIF1 α in EC, which acts through a similar mechanism through binding to the ODD domain. Although ligand activation of PPAR δ reduces the association of HIF1 α , HIF1 α is unlikely to be a co-repressor acting like Cry1/2 [28], because unlike Cry1/2, silencing of HIF1 α did not increase PPAR δ target gene expression. Quite the contrary, HIF1 α upregulated PPAR δ , suggesting that HIF1 α acts as co-activator of PPAR δ , whereas ligand activation of PPAR δ does not facilitate HIF1 α stabilization and transactivation.

In conclusion, we showed a central role of endothelial PPAR δ in vascular homeostasis and post-ischemic vascular repair by regulating gene regulatory network involved in angiogenesis, endothelial barrier function, and vascular inflammation. PPAR δ is induced by hypoxia in endothelial cells and it reciprocally enhances HIF1 α stability and transactivation. These results also provide new information about a ligand independent activation of PPAR δ in vasculature through its interaction with HIF1 α , in response to hypoxic stress.

Abbreviations

AAV: adeno-associated virus; BMEC: brain microvascular endothelial cell; CHX: cycloheximide; DBD: DNA-binding domain; EC: Endothelial cell; FITC: Fluorescein isothiocyanate; GA: gastrin; HIF1 α : hypoxia-inducible factor 1-alpha; HLI: hindlimb ischemia; LBD: ligand-binding domain; ODD: oxygen dependent degradation domain; PAD: peripheral artery disease; PPAR δ : peroxisome proliferator activated Receptor delta.

Supplementary Material

Supplementary figures and tables.

<https://www.thno.org/v12p1855s1.pdf>

Acknowledgements

We thank Prof. Chao Wan from CUHK for advice on HIF1 α , and Mr. Eric Yau, Ms. Corrina Au, Mr. Francis Chen, and Ms. Angel Fung for their technical help. This study was sponsored by the grants 81922078, 32071145 and 91739103 from National Natural Science Foundation of China; the ECS 24122318, GRF 14109519 from the Hong Kong Research Grant Council, the HMRF 05162906 from

Hong Kong Food and Health Bureau, the start-up funding, to support XYT; the CRF C4024-16W, and RIF R4012-18 from the Hong Kong Research Grant Council to support YH and RCWM.

Author contribution

YW and XYT conceived and designed the project. YW performed most of the experiments and analyzed the data. XT performed molecular cloning. SL, HH, XC, CWL performed animal experiments. RCWM, YH, KOL, XYT discussed and interpreted the data. AC and KOL provided critical reagents. YW and XYT wrote the manuscript.

Ethical Approval

All animal experiments were approved by and were performed in the designated facilities accredited by the Animal Experimental Ethics Committee of the Chinese University of Hong Kong (approval number: 19-058-HMF and 20-073-GRF), and all the animal procedures were performed in the designated facilities accredited by the Animal Experimental Ethics Committee.

Competing Interests

The authors have declared that no competing interest exists.

References

- Fowkes FG, Rudan D, Rudan I, Aboyans V, Denenberg JO, McDermott MM, et al. Comparison of global estimates of prevalence and risk factors for peripheral artery disease in 2000 and 2010: a systematic review and analysis. *Lancet*. 2013; 382: 1329-40.
- Cooke JP, Losordo DW. Modulating the vascular response to limb ischemia: angiogenic and cell therapies. *Circ Res*. 2015; 116: 1561-78.
- Gupta NK, Armstrong EJ, Parikh SA. The current state of stem cell therapy for peripheral artery disease. *Curr Cardiol Rep*. 2014; 16: 447.
- Hamik A, Wang B, Jain Mukesh K. Transcriptional Regulators of Angiogenesis. *Arteriosclerosis, Thrombosis, and Vascular Biology*. 2006; 26: 1936-47.
- Park C, Lee TJ, Bhang SH, Liu F, Nakamura R, Oladipupo SS, et al. Injury-Mediated Vascular Regeneration Requires Endothelial ER71/ETV2. *Arterioscler Thromb Vasc Biol*. 2016; 36: 86-96.
- Fan Y, Lu H, Liang W, Garcia-Barrio Minerva T, Guo Y, Zhang J, et al. Endothelial TFEB (Transcription Factor EB) Positively Regulates Postischemic Angiogenesis. *Circulation Research*. 2018; 122: 945-57.
- Bosch-Marce M, Okuyama H, Wesley Jacob B, Sarkar K, Kimura H, Liu Ye V, et al. Effects of Aging and Hypoxia-Inducible Factor-1 Activity on Angiogenic Cell Mobilization and Recovery of Perfusion After Limb Ischemia. *Circulation Research*. 2007; 101: 1310-8.
- Milkiewicz M, Pugh CW, Egginton S. Inhibition of endogenous HIF inactivation induces angiogenesis in ischaemic skeletal muscles of mice. *The Journal of Physiology*. 2004; 560: 21-6.
- Dunn Louise L, Kong Stephanie MY, Tumanov S, Chen W, Cantley J, Ayer A, et al. Hmox1 (Heme Oxygenase-1) Protects Against Ischemia-Mediated Injury via Stabilization of HIF-1 α (Hypoxia-Inducible Factor-1 α). *Arteriosclerosis, Thrombosis, and Vascular Biology*. 0: ATVBAHA.120.315393.
- Watanabe Y, Murdoch CE, Sano S, Ido Y, Bachschmid MM, Cohen RA, et al. Glutathione adducts induced by ischemia and deletion of glutaredoxin-1 stabilize HIF-1 α and improve limb revascularization. *Proc Natl Acad Sci U S A*. 2016; 113: 6011-6.
- Yin KJ, Deng Z, Hamblin M, Zhang J, Chen YE. Vascular PPARdelta protects against stroke-induced brain injury. *Arterioscler Thromb Vasc Biol*. 2011; 31: 574-81.
- Barish GD, Atkins AR, Downes M, Olson P, Chong LW, Nelson M, et al. PPARdelta regulates multiple proinflammatory pathways to suppress atherosclerosis. *Proc Natl Acad Sci U S A*. 2008; 105: 4271-6.
- Tian XY, Wong WT, Wang N, Lu Y, Cheang WS, Liu J, et al. PPARdelta activation protects endothelial function in diabetic mice. *Diabetes*. 2012; 61: 3285-93.

14. Fan Y, Wang Y, Tang Z, Zhang H, Qin X, Zhu Y, et al. Suppression of pro-inflammatory adhesion molecules by PPAR-delta in human vascular endothelial cells. *Arterioscler Thromb Vasc Biol.* 2008; 28: 315-21.
15. Graham TL, Mookherjee C, Suckling KE, Palmer CN, Patel L. The PPARdelta agonist GW0742X reduces atherosclerosis in LDLR(-/-) mice. *Atherosclerosis.* 2005; 181: 29-37.
16. Li AC, Binder CJ, Gutierrez A, Brown KK, Plotkin CR, Pattison JW, et al. Differential inhibition of macrophage foam-cell formation and atherosclerosis in mice by PPARalpha, beta/delta, and gamma. *J Clin Invest.* 2004; 114: 1564-76.
17. Piqueras L, Reynolds AR, Hodivala-Dilke KM, Alfranca A, Redondo JM, Hatae T, et al. Activation of PPARbeta/delta induces endothelial cell proliferation and angiogenesis. *Arterioscler Thromb Vasc Biol.* 2007; 27: 63-9.
18. He T, Lu T, d'Uscio LV, Lam CF, Lee HC, Katusic ZS. Angiogenic function of prostacyclin biosynthesis in human endothelial progenitor cells. *Circ Res.* 2008; 103: 80-8.
19. He T, Smith LA, Lu T, Joyner MJ, Katusic ZS. Activation of peroxisome proliferator-activated receptor-[delta] enhances regenerative capacity of human endothelial progenitor cells by stimulating biosynthesis of tetrahydrobiopterin. *Hypertension.* 2011; 58: 287-94.
20. Han JK, Lee HS, Yang HM, Hur J, Jun SI, Kim JY, et al. Peroxisome proliferator-activated receptor-delta agonist enhances vasculogenesis by regulating endothelial progenitor cells through genomic and nongenomic activations of the phosphatidylinositol 3-kinase/Akt pathway. *Circulation.* 2008; 118: 1021-33.
21. Liou JY, Lee S, Ghelani D, Matijevic-Aleksic N, Wu KK. Protection of endothelial survival by peroxisome proliferator-activated receptor-delta mediated 14-3-3 upregulation. *Arterioscler Thromb Vasc Biol.* 2006; 26: 1481-7.
22. Baker M, Robinson SD, Lechertier T, Barber PR, Tavora B, D'Amico G, et al. Use of the mouse aortic ring assay to study angiogenesis. *Nat Protoc.* 2011; 7: 89-104.
23. Carpentier G, Berndt S, Ferratge S, Rasband W, Cuendet M, Uzan G, et al. Angiogenesis Analyzer for ImageJ - A comparative morphometric analysis of "Endothelial Tube Formation Assay" and "Fibrin Bead Assay". *Sci Rep.* 2020; 10: 11568.
24. Yan Q, Bartz S, Mao M, Li L, Kaelin WG, Jr. The hypoxia-inducible factor 2alpha N-terminal and C-terminal transactivation domains cooperate to promote renal tumorigenesis in vivo. *Mol Cell Biol.* 2007; 27: 2092-102.
25. Koshiji M, Kageyama Y, Pete EA, Horikawa I, Barrett JC, Huang LE. HIF-1alpha induces cell cycle arrest by functionally counteracting Myc. *EMBO J.* 2004; 23: 1949-56.
26. Emerling BM, Weinberg F, Liu JL, Mak TW, Chandel NS. PTEN regulates p300-dependent hypoxia-inducible factor 1 transcriptional activity through Forkhead transcription factor 3a (FOXO3a). *Proc Natl Acad Sci U S A.* 2008; 105: 2622-7.
27. Chen W, Hill H, Christie A, Kim MS, Holloman E, Pavia-Jimenez A, et al. Targeting renal cell carcinoma with a HIF-2 antagonist. *Nature.* 2016; 539: 112-7.
28. Jordan SD, Kriebs A, Vaughan M, Duglan D, Fan W, Henriksson E, et al. CRY1/2 Selectively Repress PPARdelta and Limit Exercise Capacity. *Cell Metab.* 2017; 26: 243-55 e6.
29. Nelson JD, Denisenko O, Bomsztyk K. Protocol for the fast chromatin immunoprecipitation (ChIP) method. *Nat Protoc.* 2006; 1: 179-85.
30. Brenes RA, Jadlovec CC, Bear M, Hashim P, Prottack CD, Li X, et al. Toward a mouse model of hind limb ischemia to test therapeutic angiogenesis. *J Vasc Surg.* 2012; 56: 1669-79; discussion 79.
31. Sluiter TJ, van Buul JD, Huveneers S, Quax PHA, de Vries MR. Endothelial Barrier Function and Leukocyte Transmigration in Atherosclerosis. *Biomedicines.* 2021; 9.
32. Rey S, Semenza GL. Hypoxia-inducible factor-1-dependent mechanisms of vascularization and vascular remodelling. *Cardiovasc Res.* 2010; 86: 236-42.
33. Chen C, Pore N, Behrooz A, Ismail-Beigi F, Maity A. Regulation of glut1 mRNA by hypoxia-inducible factor-1. Interaction between H-ras and hypoxia. *J Biol Chem.* 2001; 276: 9519-25.
34. Semenza GL. Hypoxia-inducible factor 1 (HIF-1) pathway. *Sci STKE.* 2007; 2007: cm8.
35. Yu B, Miao ZH, Jiang Y, Li MH, Yang N, Li T, et al. c-Jun protects hypoxia-inducible factor-1alpha from degradation via its oxygen-dependent degradation domain in a nontranscriptional manner. *Cancer Res.* 2009; 69: 7704-12.
36. Ivan M, Kondo K, Yang H, Kim W, Valiano J, Ohh M, et al. HIFalpha targeted for VHL-mediated destruction by proline hydroxylation: implications for O2 sensing. *Science.* 2001; 292: 464-8.
37. Piqueras L, Reynolds Andrew R, Hodivala-Dilke Kairbaan M, Alfranca A, Redondo Juan M, Hatae T, et al. Activation of PPARbeta/delta Induces Endothelial Cell Proliferation and Angiogenesis. *Arteriosclerosis, Thrombosis, and Vascular Biology.* 2007; 27: 63-9.
38. Ho SY, Kwan YP, Qiu B, Tan A, Murray HL, Barathi VA, et al. Investigating the Role of PPARbeta/delta in Retinal Vascular Remodeling Using Pparbeta/delta-Deficient Mice. *Int J Mol Sci.* 2020; 21.
39. Chehaibi K, le Maire L, Bradoni S, Escola JC, Blanco-Vaca F, Slimane MN. Effect of PPAR-beta/delta agonist GW0742 treatment in the acute phase response and blood-brain barrier permeability following brain injury. *Translational Research.* 2017; 182: 27-48.
40. Suarez S, McCollum GW, Bretz CA, Yang R, Capozzi ME, Penn JS. Modulation of VEGF-Induced Retinal Vascular Permeability by Peroxisome Proliferator-Activated Receptor-beta/delta. *Investigative Ophthalmology & Visual Science.* 2014; 55: 8232-40.
41. d'Uscio LV, He T, Santhanam AVR, Tai L-J, Evans RM, Katusic ZS. Mechanisms of vascular dysfunction in mice with endothelium-specific deletion of the PPAR-delta gene. *American Journal of Physiology-Heart and Circulatory Physiology.* 2014; 306: H1001-H10.
42. Inoue T, Kohro T, Tanaka T, Kanki Y, Li G, Poh H-M, et al. Cross-enhancement of ANGPTL4 transcription by HIF1 alpha and PPAR beta/delta is the result of the conformational proximity of two response elements. *Genome Biology.* 2014; 15: R63.
43. Rey S, Lee K, Wang CJ, Gupta K, Chen S, McMillan A, et al. Synergistic effect of HIF-1alpha gene therapy and HIF-1-activated bone marrow-derived angiogenic cells in a mouse model of limb ischemia. *Proc Natl Acad Sci U S A.* 2009; 106: 20399-404.
44. Oladipupo S, Hu S, Kovalski J, Yao J, Santeford A, Sohn RE, et al. VEGF is essential for hypoxia-inducible factor-mediated neovascularization but dispensable for endothelial sprouting. *Proceedings of the National Academy of Sciences.* 2011; 108: 13264.
45. Huang X, Zhang X, Zhao DX, Yin J, Hu G, Evans CE, et al. Endothelial Hypoxia-Inducible Factor-1alpha Is Required for Vascular Repair and Resolution of Inflammatory Lung Injury through Forkhead Box Protein M1. *The American Journal of Pathology.* 2019; 189: 1664-79.
46. Lee SH, Che X, Jeong JH, Choi JY, Lee YJ, Lee YH, et al. Runx2 protein stabilizes hypoxia-inducible factor-1alpha through competition with von Hippel-Lindau protein (pVHL) and stimulates angiogenesis in growth plate hypertrophic chondrocytes. *J Biol Chem.* 2012; 287: 14760-71.
47. Li J, Xu Y, Long XD, Wang W, Jiao HK, Mei Z, et al. Cbx4 governs HIF-1alpha to potentiate angiogenesis of hepatocellular carcinoma by its SUMO E3 ligase activity. *Cancer Cell.* 2014; 25: 118-31.